RSC Advances

ROYAL SOCIETY OF CHEMISTRY

www.rsc.org/advances

Controllable multicolor output, white luminescence and cathodoluminescence properties of high quality $NaCeF_4:Ln^{3+}$ (Ln^{3+} = Eu^{3+}, Dy^{3+}, Tb^{3+}) nanorods

*Zhigao Yi,[a,b] Wei Lu,[c] Tianmei Zeng,[a] Chao Qian,[a] Haibo Wang,[a,b] Ling Rao,[a,b] Hongrong Liu,[a] and Songjun Zeng [*a]*

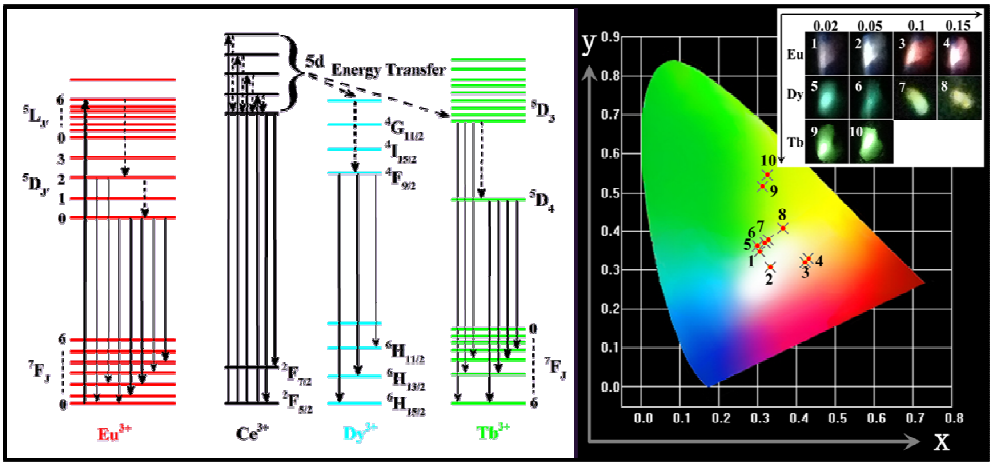

Tunable multicolor and white emissions of hexagonal phase lanthanides (Ln^{3+}, Ln^{3+} = Eu^{3+}, Dy^{3+}, Tb^{3+}) doped $NaCeF_4$ nanorods with uniformed morphology and monodispersity synthesized via a hydrothermal method.

Cite this: DOI: 10.1039/c0xx00000x

www.rsc.org/xxxxxx

ARTICLE TYPE

Controllable multicolor output, white luminescence and cathodoluminescence properties of high quality $NaCeF_4:Ln^{3+}$ (Ln^{3+} = Eu^{3+}, Dy^{3+}, Tb^{3+}) nanorods

Zhigao Yi,[a,b] Wei Lu,[c] Tianmei Zeng,[a] Chao Qian,[a] Haibo Wang,[a,b] Ling Rao,[a,b] Hongrong Liu,[a] and Songjun Zeng[*a]

Received (in XXX, XXX) Xth XXXXXXXXX 20XX, Accepted Xth XXXXXXXXX 20XX
DOI: 10.1039/b000000x

Herein, a series of hexagonal phase lanthanides (Ln^{3+}, Ln^{3+} = Eu^{3+}, Dy^{3+}, Tb^{3+}) doped $NaCeF_4$ nanorods (NRs) with uniformed morphology and monodispersity have been successfully synthesized via a typical hydrothermal method using oleic acid as capping agent. The crystal phase and microstructure of the obtained NRs were analyzed by X-ray diffraction (XRD) patterns and transmission electron microscopy (TEM). The downconversion (DC) luminescence properties and mechanisms of the as-prepared $NaCeF_4:Ln^{3+}$ NRs have been discussed in detail. The as-prepared samples show the characteristic f-f transition of Ln^{3+} (Ln^{3+} = Eu^{3+}, Dy^{3+}, Tb^{3+}), respectively. The decay time and quantum yield of these obtained NRs are also studied. Moreover, tunable multicolor, especially white emissions can be successfully achieved via varying the doping ions and doping concentration. With increasing the contents of Eu^{3+}, the emission colors vary from light green to white and finally to light red under the excitation of 395 nm. The calculated CIE coordinates of the obtained white emissions are (0.33, 0.31), which are exactly closed to the standard white light located at (0.33, 0.33). This is the first time for achieving white light emission via only single-doping Eu^{3+} into $NaCeF_4$ system. In addition, the multicolor output changing from yellowish green to yellow under the excitation at 261 nm was also obtained by only tuning the doped contents of Dy^{3+} in $NaCeF_4$ host. As for Tb^{3+}, bright yellowish green emissions were obtained under the excitation at 261 nm. Besides, the cathodoluminescence (CL) spectra demonstrated that these NRs can emerge as ideal nanophosphors under electron beam excitation. Therefore, the as-prepared $NaCeF_4:Ln^{3+}$ NRs with tunable multicolor output and bright white emissions might be applied in field-emission devices, multicolor display and solid state laser.

1. Introduction

In recent years, much more attentions have been received on shape and size controlled synthesis of Ln^{3+} doped nanocrystals,[1-18] because of their shape/size dependent properties and potential applications in optics, laser, light emitting devices, and biological labeling/imaging, etc. It is illustrated that the morphology and size of nanocrystals have great influence on their physical and chemical properties.[19] Thus, the controlled fabrication of Ln^{3+}-doped nanomaterials with favorable shapes and sizes is of much significance.

The Ln^{3+}-doped nanocrystals exhibit excellent photoluminescence (PL) capabilities owing to the two different energy transfer mechanisms, namely, upconversion[20-29] (UC) and DC[30-40] process. DC generation is the one which converts higher-energy radiation to lower-energy photon emissions,[1,2] while the UC process is the exactly opposite process. Among all the exploited Ln^{3+}-doped nanocrystals, fluorides ($NaLnF_4$), are considered as the most efficient lattice hosts. However, the Ln^{3+}-doped nanocrystals using $NaCeF_4$ as host matrix and high quality $NaCeF_4$ nanocrystals with monodispersity are still rare reported. In contrast to the well-established $NaYF_4$ host, $NaCeF_4$ system we selected here can serve as not only perfect host materials but also activator, which makes it simpler to obtain the multicolor output and intense white emissions by single doping Ln^{3+} in a system. Apart from the advantages of PL properties, the price of cerium oxide as raw materials used in our experiments is quite reasonable than other oxides.[41] As previously reported, CeF_3 and $NaCeF_4$ nanocrystals were synthesized through the liquid-solid-solution approach by Li et al,[41] in which the emphasis focused on the nucleation and growth of the nanocrystals and didn't reveal the effect of Ln^{3+} doping on their PL property. In addition, the $NaCeF_4$ nanoparticles with different shape and size were obtained by using the solvothermal method via tuning the pH value and sodium concentration in the solution.[36] However, the as-prepared $NaCeF_4$ nanoparticles are irregular and not uniform. Recently, hexagonal phase $NaCeF_4$ NRs were successfully fabricated via the polyol-mediated solvothermal route by Qu et al.[37] The major work contributed to achieve varied morphology and size of $NaCeF_4$ nanocrystals by regulating the additive contents of NH_4F

and $NaNO_3$. Therefore, it is important to develop a proper method and experimental parameters to achieve hexagonal phase $NaCeF_4$ nanocrystals with uniform shape and monodispersity. Besides, the systematic study on the DC luminescence of the Ln^{3+}-doped $NaCeF_4$ nanocrystals is of significance. In addition, many recent literatures[30-33] have focused on the phosphors which co-doped with Ce^{3+}, Mn^{2+}, Eu^{3+}, Dy^{3+}, and Tb^{3+} to obtain tunable multicolor emission, even white light for application in light emitting devices. The efficient and intense energy transfer from Ce^{3+} to Mn^{2+}/Dy^{3+}/Tb^{3+} in these phosphors have been systematic studied. However, white emissions obtained by the single doping of Ln^{3+} into the hosts still remain great challenges and there are few reports in Ln^{3+} doped $NaCeF_4$ nanocrystals.

In this paper, high quality and monodispersed hexagonal phase $NaCeF_4$ NRs doped with different contents of Ln^{3+} (Ln^{3+} = Eu^{3+}, Dy^{3+}, and Tb^{3+}) were successfully prepared via a hydrothermal method. The crystal phase and microstructure of the as-prepared Ln^{3+} doped $NaCeF_4$ NRs were characterized by XRD and TEM, respectively. The PL properties were recorded by the excitation, emission spectra and the corresponding energy transfer mechanisms were discussed in detail. Interestingly, the tunable multicolor and especially white emissions are obtained by only changing the content of single-doped ions in $NaCeF_4$ host.

2. Experimental

2.1 Chemicals and Materials

All the rare earth oxides (Sigma-Aldrich) were 99.99% of purity and other chemicals (Sinopharm Chemical Reagent Co., China) were of analytical grade and used as received without further purification. $Ln(NO_3)_3$ (Ln = Ce^{3+}, Eu^{3+}, Dy^{3+}, and Tb^{3+}) solutions of 0.5 M were prepared via dissolving the corresponding rare earth oxides into dilute nitric acid at temperature of 80 °C, respectively.

2.2 Synthesis of the high quality Ln^{3+}-doped $NaCeF_4$ NRs

High quality and monodispersed $NaCeF_4$ NRs doped with different contents of Ln^{3+} were synthesized through a hydrothermal procedure by using oleic acid as stabilizing agent.[41-44] In a typical synthesis, 1.2 g of NaOH was dissolved in 2 mL of deionized water and then 10 mL of ethanol and 20 mL of oleic acid were added under vigorously stirring to obtain a transparent homogeneous solution. After stirring for 30 min, total amounts (1 mmol) of $Ln(NO_3)_3$ (Ln = Ce^{3+}, Eu^{3+}, Dy^{3+}, and Tb^{3+}) with designed composition were added into the aforementioned solution under vigorous agitation. After that, 6 mL of NaF aqueous solution (1 M) was added, and the resulting mixture was stirred vigorously for another 20 min. Finally, the obtained mixture was sealed and kept at 190 °C for 24 h by transferring into a 50 mL stainless Teflon-lined autoclave. Cool the system naturally to room temperature after reaction. The products were deposited at the bottom of the vessel. The as-prepared samples were separated by centrifugation and washed several times with ethanol and deionized water to remove oleic acid and other remnants, and then, dried at 60 °C in air for 24 h.

2.3 Characterizations

The crystal phase compositions of the as-prepared $NaCeF_4$ NRs doped with different contents of Dy^{3+} were examined by XRD utilizing a D/max-γA system X-ray diffractometer at 40 kV and 250 mA with Cu Kα radiation (λ = 1.54056 Å). The microstructures of the as-prepared samples were characterized by TEM, scanning TEM (STEM), selective area electron diffraction (SAED) patterns and high-resolution TEM (HR-TEM) via a JEM-2100F TEM equipped with an energy-dispersive X-ray spectroscopy (EDS) system using an accelerating voltage at 200 kV. The obtained samples for TEM assays were prepared as follows: 0.1 mg of the as-prepared samples were dispersed in 1 mL of cyclohexane solvent to form a homogeneous colloidal mixture, and then one drop of the suspension was added on the TEM copper grid covered with carbon film. The DC luminescence excitation/emission spectra and decay time profile were recorded by a Zolix Analytical Instrument (fluoroSENS 9000A). The decaytime curves of the samples were recorded using the Zolix Analytical Instrument by monitoring the correspnding strongest excitation and emission wavelengths (excitation/emission bandpass: 8 mm, integrate time: 200 μs). The quantum yields of the Ln-doped $NaCeF_4$ NRs were measured by the affiliated quantum yield measurement system of the spectroscope, in which an integrating sphere as a sample chamber. The digital photographs of the as-prepared Ln-doped $NaCeF_4$ samples were taken by a Canon digital camera under the strongest excitation at the corresponding wavelength. A cathodoluminescence spectrometer (Gantan MonoCL3+) equipped on the environmental scanning electron microscopy (Quanta 400 FEG, FEI) was used to measure the CL spectra of the samples (accelerating voltage of electron beam: 3.15 kV for $NaCeF_4$:Eu^{3+}, 4.75 kV for $NaCeF_4$:Dy^{3+}/Tb^{3+}).

3. Results and Discussion

3.1 Phase and Microstructure study

The crystal structure of $ALnF_4$ exhibits two polymorphic forms (cubic and hexagonal phases), depending on the selected synthesis conditions and methods. It has been illustrated that the hexagonal phase $ALnF_4$ is a much better host lattice than the cubic counterpart for the UC/DC luminescence.[45] Usually, in order to obtain the pure hexagonal phase $ALnF_4$, sufficiently higher temperature and longer time are needed for reaction. Figure 1 shows the XRD patterns of the as-prepared Dy^{3+} doped $NaCeF_4$ NRs via the hydrothermal procedure at 190 °C for 24 h. It can be seen that all the diffraction peaks of the products can be well indexed to the pure hexagonal phase $NaCeF_4$ structure (JCPDS, number 50-0154). Besides, the diffraction peaks of the products are very sharp and strong, indicating the formation of the $NaCeF_4$ samples with high crystallinity through this method. In addition, one can observe from the red dotted line that the diffraction peaks of the $NaCeF_4$:Dy^{3+} samples shifted toward high angles gradually with increasing the doping contents of Dy^{3+}, indicating the decrease of unit-cell volume. This is mainly ascribed to the smaller ionic radius of Dy^{3+} (r = 1.167 Å) to replace the relatively larger Ce^{3+} (r = 1.283 Å).[46] Moreover, the broadened diffraction peaks reveals that the average crystalline size decreases with increasing the contents of Dy^{3+}. It should be noted that the Eu^{3+} and Tb^{3+} doped samples present the similar results (data not shown).

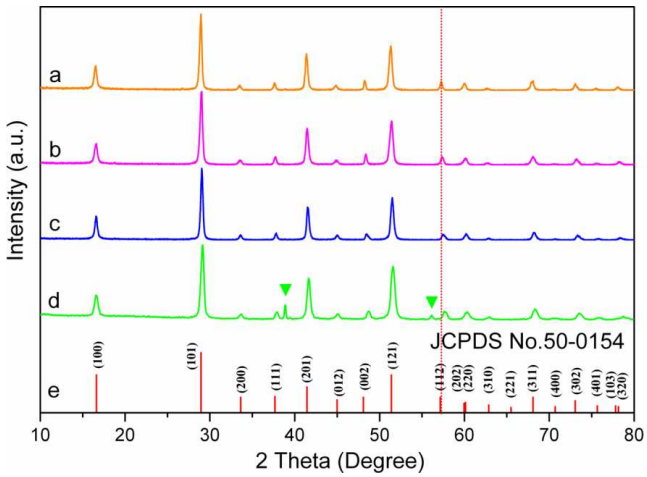

Figure 1. Typical XRD patterns of the $NaCeF_4$ NRs doped with different Dy^{3+} contents: a) 0.02, (b) 0.05, (c) 0.1, and (d) 0.15, (e) the standard hexagonal phase $NaCeF_4$ (JCPDS number: 50-0154). The diffraction peaks of the residual NaF were indicated by green triangles. The peaks shift towards higher angles (marked by a red dotted line).

To investigate the morphology and size of $NaCeF_4$:mDy^{3+} NRs, further TEM and STEM characterizations have been performed and the results are shown in Figure 2. As demonstrated, all of the samples present highly monodispersed and uniformed NRs and can be self-assembled into a two-dimensional ordered array. The aspect ratios of the samples were measured to be 8.02, 9.41, and 13.59, respectively with the increase of the Dy^{3+} concentration from 0.02 to 0.10. This size evolution is due to the effect of the Dy^{3+} dopant ion on crystal growth rate through surface charge modification.[7] Liu's[7] and our previous reports[42] reveal that the crystal size can be readily tuned by doping Ln^{3+} with different ion radius in $NaLnF_4$ host. The smaller Ln^{3+} dopants may result in the formation of larger sized nanocrystal. Therefore, in our case, the increased size is mainly attributed to the doped Ln^{3+} (Dy^{3+}) with larger ion radius.

The HR-TEM and SAED results (right panels in Figure 2) show that the as-prepared NRs present high crystallinity and single crystal nature. The interplanar crystal spacing of [002] and [200] lattice planes measured from HR-TEM results (right panels in Figure 2) decreased gradually when the Dy^{3+} doping content varying from 0.02 to 0.15, which is well coincident with the analyzed results of the XRD patterns. Moreover, the preferred growth direction is along the [001] direction. During the STEM analysis, the corresponding EDS and EDS mapping have been obtained and the results of the $NaCeF_4$:0.05Dy^{3+} NRs present in Figure 3. The EDS result (Figure 3f) reveals that the as-prepared $NaCeF_4$:0.05Dy^{3+} NRs are mainly composed of Na^+, Ce^{3+}, F^-, Dy^{3+} and no other impurity has been detected. Further EDS mappings show that the elements (Na^+, Ce^{3+}, F^-, Dy^{3+}) are uniformly dispersed within the regions of the NRs. Similar with the Dy^{3+} doped $NaCeF_4$, the Eu^{3+} or Tb^{3+} doped samples also exhibit highly uniformed and monodispersed NRs (data not shown).

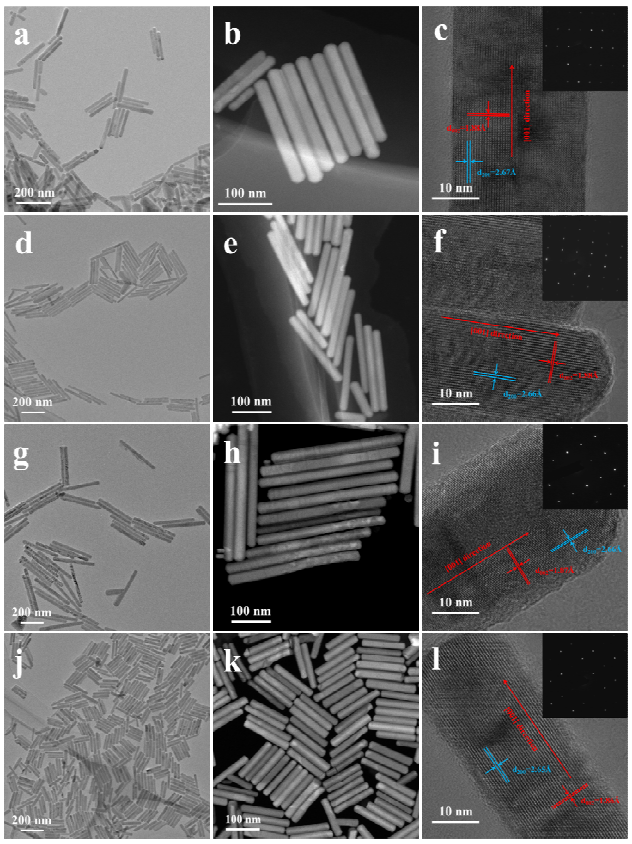

Figure 2. TEM (left panel), STEM (middle panel), and HR-TEM (right panel) images of the $NaCeF_4$ NRs doped with different contents of Dy^{3+}: (a) 0.02, (d) 0.05, (g) 0.1, and (j) 0.15. The right-up inset of each HR-TEM image shows the corresponding SAED pattern.

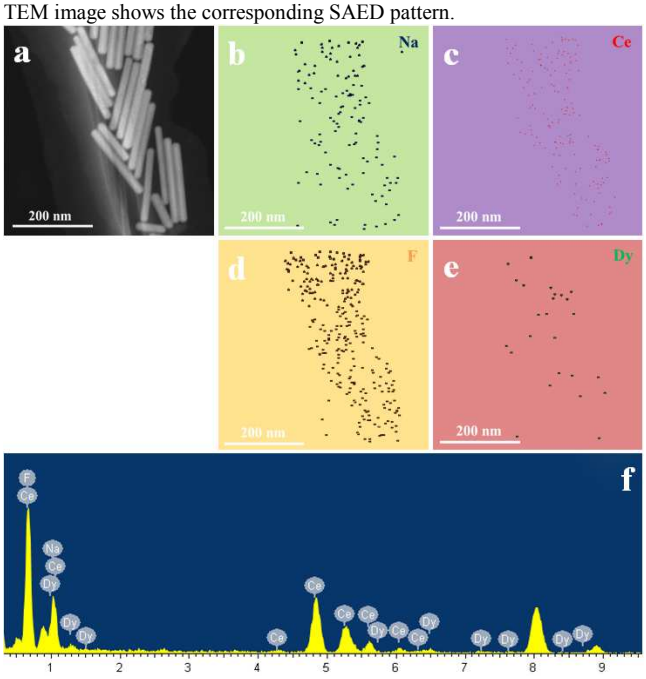

Figure 3. (a) STEM of the $NaCeF_4$:0.05Dy NRs, (b-e) the corresponding EDS mapping of as-prepared NRs shown in a, and (f) EDS of the $NaCeF_4$:0.05Dy^{3+} samples.

3.2 Tunable Multicolor and DC Properties

As a doping ion, Eu^{3+} concentration in host has great influence on the emission intensity and the shapes of the spectra.[38] Therefore,

we herein selected a series of doping contents of Eu^{3+} (0.02, 0.05, 0.1, and 0.15) to investigate the spectral and luminescence nature in the hexagonal $NaCeF_4$ host lattice. Figure 4 shows the excitation and emission spectra of Eu^{3+} doped $NaCeF_4$ NRs. As presented in Figure 4a, the excitation spectra contain characteristic peaks of Eu^{3+} within the configuration $^4F_6$ between 250 and 450 nm, which is analogous to the absorption curve for Eu^{3+} in the YF_3 and $NaYF_4$ host.[39] The excitation lines can be attributed to the corresponding energy transfer: (317 nm, $^7F_0 \rightarrow {}^5H_6$; 361 nm, $^7F_0 \rightarrow {}^5D_4$; 384 nm, $^7F_0 \rightarrow {}^5G_2$; 395 nm, $^7F_0 \rightarrow {}^5L_6$, strongest; and 415 nm, $^7F_0 \rightarrow {}^5D_3$). In addition, these weak lines (such as 253, 286, and 297 nm) have little contribution to the emission. The excitation spectra of these Eu^{3+} ions in $NaCeF_4$ host have much difference from that in oxides host, where the charge-transfer band (200-300 nm) of Eu^{3+}-O^{2-} has been detected constantly. In comparison with Ce^{3+}/Dy^{3+} and Ce^{3+}/Tb^{3+} co-doped nanomaterials, the combination between $Eu^{3+}$and Ce^{3+} also exhibits distinctive excitation property which can be attributed to the transitions of the different crystal field splitting levels of the 5d state for Ce^{3+} ions in the $NaCeF_4$ host.

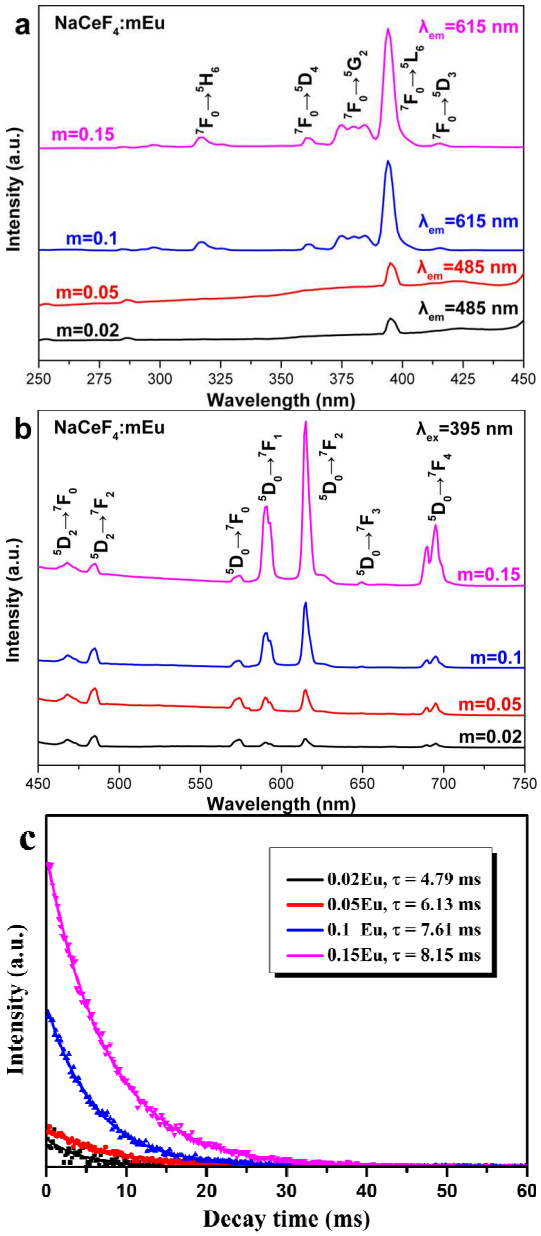

Figure 4. (a) Excitation and (b) emission spectra of $NaCeF_4$:mEu^{3+} (m = 0.02, 0.05, 0.1, and 0.15) NRs. (c) luminescence decay (λ_{ex} = 395 nm, λ_{em} = 615 nm) spectra of $NaCeF_4$:mEu^{3+} NRs.

The luminescent intensities of the $NaCeF_4$:Eu^{3+} NRs were remarkably enhanced via increasing the doping contents of Eu^{3+} from 0.02 to 0.15 (Figure 4b). As demonstrated in Figure 4b, the emission spectra of the $NaCeF_4$:mEu^{3+} NRs were obtained by the strongest excitation wavelength of 395 nm ($^7F_0 \rightarrow {}^5L_6$ transition of Eu^{3+}). According to the proposed energy level diagram (Figure 5), all the emission lines are composed of $^5D_{0,2} \rightarrow {}^7F_J$ transitions of Eu^{3+}, namely, 468 nm, $^5D_2 \rightarrow {}^7F_0$; 485 nm, $^5D_2 \rightarrow {}^7F_2$; 574 nm, $^5D_0 \rightarrow {}^7F_0$; 591 nm, $^5D_0 \rightarrow {}^7F_1$; 615 nm, $^5D_0 \rightarrow {}^7F_2$; 649 nm, $^5D_0 \rightarrow {}^7F_3$; and 690/695 nm, $^5D_0 \rightarrow {}^7F_4$.[36] In comparison to the PL properties of the Dy^{3+} and Tb^{3+} doped $NaCeF_4$ system, the Eu^{3+} doped $NaCeF_4$ NRs present very weak excitation peak centered at 261 nm of Ce^{3+}, indicating the intense emissions of the as-prepared $NaCeF_4$:Eu^{3+} NRs come from the intrinsic emissions of the Eu^{3+} rather than the energy transfer between Ce^{3+} and Eu^{3+}. Moreover, with increasing Eu^{3+} contents, the excitation peak centered at 261 nm of Ce^{3+} is gradually disappeared, indicating the hardness of direct sensitization of Eu^{3+} by Ce^{3+}, which is similar with the previous report.[47] This is mainly ascribed to the electron transfer quenching effect between Ce^{3+} and Eu^{3+}, resulting in poor energy transfer from Ce^{3+} to Eu^{3+}.[47-49] The energy transfer probability depends on the critical distance of energy transfer.[50,51] As demonstrated from Figure 4b, the relative emission intensity ratio of the transitions ($^5D_2 \rightarrow {}^7F_J$)/($^5D_0 \rightarrow {}^7F_J$) decreased when increasing the doping contents of Eu^{3+}. Besides, the strongest emission peak of Eu^{3+} is not constant, which centered at 485 nm when the doping content of Eu^{3+} in $NaCeF_4$ host is low (0.02 and 0.05) and centered at 615 nm while the Eu^{3+} composition increasing to 0.1 and 0.15. In general, the differences in relative emission intensity are mainly attributed to the doping contents of Eu^{3+} and their predominant vibration frequencies available in the host.[40] In addition, the emission peaks centered at 591 nm ($^5D_0 \rightarrow {}^7F_1$) and 615 nm ($^5D_0 \rightarrow {}^7F_2$) are ascribed to magnetic and electric dipole transitions of Eu^{3+}, respectively, and the asymmetric environment of the Eu^{3+} ion in the host can be calculated by the integrated intensity ratio (denoted as A_{21}) of electric to magnetic dipole transitions.[52-54] The A_{21} values are calculated to be ~ 1.47, 1.56, 1.58, and 1.80, respectively, when increasing the dopant of Eu^{3+}. The $^5D_0 \rightarrow {}^7F_2$ transition is more sensitive than that of the $^5D_0 \rightarrow {}^7F_1$ transition and the peak at 615 nm is always dominant than the one at 591 nm. The higher the A_{21} value indicates that the higher local disorder and distortion appear in the Eu^{3+} doped $NaCeF_4$ system, which can enhance the emission intensity enormously. The CIE coordinates (labeled from 1 to 4 in Figure 8) are calculated to (0.31, 0.36) for $NaCeF_4$:$0.02Eu^{3+}$, (0.33, 0.31) for $NaCeF_4$:$0.05Eu^{3+}$, (0.42, 0.32) for $NaCeF_4$:$0.1Eu^{3+}$, and (0.43, 0.33) for $NaCeF_4$:$0.15Eu^{3+}$ NPs, respectively. From the corresponding digital photographs of the powders (the insets in Figure 8), the tunable multicolor output from green to bright white and finally to red was readily obtained by single doping Eu^{3+} in $NaCeF_4$ host. Moreover, the calculated CIE coordinates (0.33, 0.31) of $NaCeF_4$:$0.05Eu^{3+}$ NRs are exactly closed to the standard white light emission (0.33, 0.33). These findings provide a new route for achieving white light emissions

by only single doping Ln^{3+}, which is different with previous reported Ce^{3+}/Mn^{2+} co-doped phosphors.[55] The PL decay profile of $^5D_0$ level at 615 nm of Eu^{3+} for these $NaCeF_4$: Eu^{3+} NRs under the excitation of 395 nm is shown in Figure 4c. The experimental data were fitted by mono-exponential function and the lifetimes were calculated to 4.79, 6.13, 7.61, and 8.15 ms. Respectively. In addition, the quantum yields of the $NaCeF_4$: Eu^{3+} NRs were measured to 33%, 40%, 49%, and 57%, respectively.

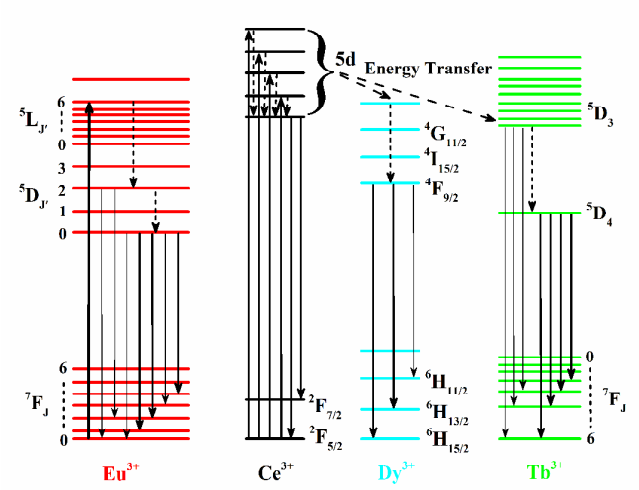

Figure 5. The proposed energy level diagram and luminescence mechanisms of the $NaCeF_4$:Ln^{3+} NRs.

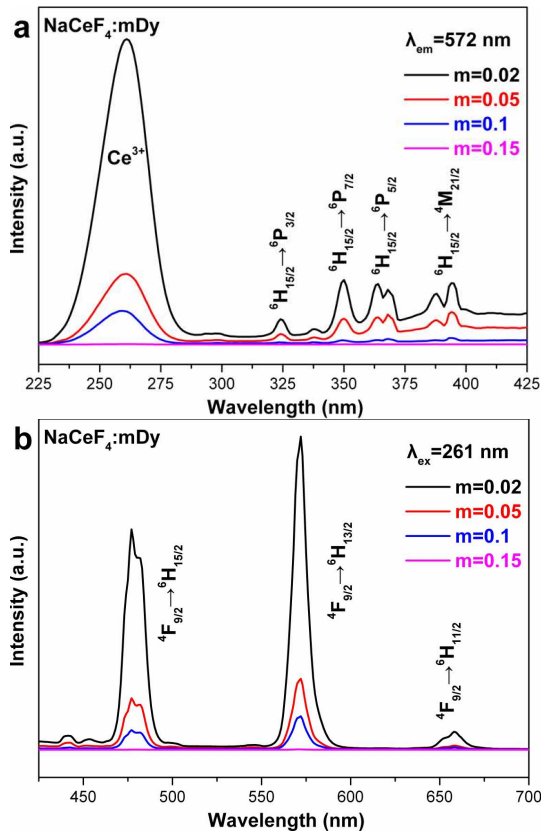

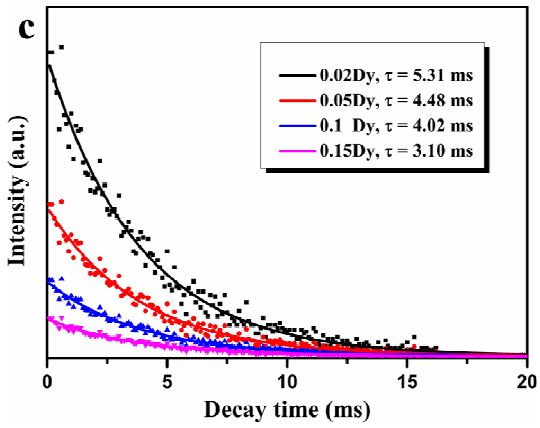

Figure 6. (a) Excitation and (b) emission spectra of $NaCeF_4$:mDy^{3+} (m = 0.02, 0.05, 0.1, and 0.15) NRs. (c) luminescence decay (λ_{ex} = 261 nm, λ_{em} = 572 nm) spectra of $NaCeF_4$:mDy^{3+} NRs.

The $NaCeF_4$:mDy^{3+} (m = 0.02, 0.05, 0.1, and 0.15) NRs also exhibit unique DC properties and the excitation/emission spectra are illustrated in Figure 6a and 6b, respectively. The excitation spectra (Figure 6a) are composed of the intense absorption band centered at 261 nm of Ce^{3+} and the relative weak characteristic f-f transition lines of Dy^{3+}, which are assigned to the corresponding energy transfer: 324 nm, $^6H_{15/2} \rightarrow {}^6P_{3/2}$; 350 nm, $^6H_{15/2} \rightarrow {}^6P_{7/2}$; 364/368 nm, $^6H_{15/2} \rightarrow {}^6P_{5/2}$; and 388/395 nm, $^6H_{15/2} \rightarrow {}^4M_{21/2}$, respectively. On the other side, the emission spectra (Figure 6b) excited via the intense Ce^{3+} absorption peaked at 261 nm are dominated by two groups of emissions (477/482 nm, $^4F_{9/2} \rightarrow {}^6H_{15/2}$; and 572 nm, $^4F_{9/2} \rightarrow {}^6H_{13/2}$). In addition, there is still some weak emission transition like $^4F_{9/2} \rightarrow {}^6H_{11/2}$ of Dy^{3+} at 658 nm. The energy transfer mechanism of Dy^{3+} in the $NaCeF_4$ matrix is shown in Figure 5. Under the UV excitation, the energy transfer took place between Ce^{3+} ions at first, and then transferred from Ce^{3+} (5d) to Dy^{3+}. Finally, the excited levels of Dy^{3+} radiatively transferred to the lower energy levels. The multicolor emissions, such as, yellowish green for $NaCeF_4$:0.02/0.05/0.1Dy^{3+} and yellow for $NaCeF_4$:0.15Dy^{3+}, are obtained under the excitation of 261 nm (insets in Figure 8). The calculated CIE coordinates followed by the emission spectra are measured to (0.30, 0.37) for $NaCeF_4$:0.02Dy^{3+}, (0.31, 0.37) for $NaCeF_4$:0.05Dy^{3+}, (0.32, 0.38) for $NaCeF_4$:0.1Dy^{3+}, and (0.36, 0.41) for $NaCeF_4$:0.15Dy^{3+} as marked from 5 to 8 in Figure 8. The PL decay profile (shown in Figure 6c) of the $NaCeF_4$:mDy^{3+} NRs also matched well with the mono-exponential curve fit and the calculated decay time are 5.31, 4.48, 4.02, and 3.10 ms, respectively, which is ascribed to the transition ($^4F_{9/2} \rightarrow {}^6H_{13/2}$). The quantum yields of the $NaCeF_4$: mDy^{3+} NRs were tested to 41%, 27%, 24%, and 13%, respectively.

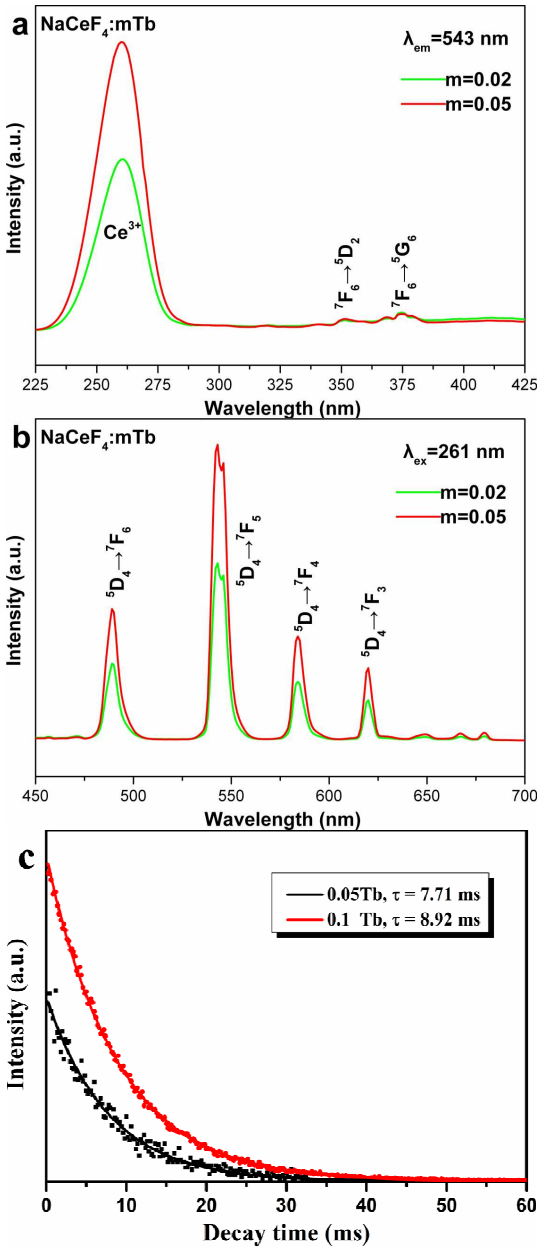

Figure 7. (a) Excitation and (b) emission spectra of $NaCeF_4$:mTb^{3+} (m = 0.02 and 0.05) NRs. (c) luminescence decay (λ_{ex} = 261 nm, λ_{em} = 543 nm) spectra of $NaCeF_4$:mTb^{3+} NRs.

As for Tb^{3+}, it contains a low energy state (^7F_J, J = 0, …, 6) and excited states ($^5D_3$ and $^5D_4$), which in general results in blue or green emissions while a low or high doping content of Tb^{3+}, respectively.[56] Similar to the Dy^{3+} doped $NaCeF_4$ samples, the excitation spectra of $NaCeF_4$:mTb^{3+} (m = 0.02 and 0.05) consist of a predominate Ce^{3+} absorption line peaked at 261 nm and relative weak f-f transitions of Tb^{3+} (351 nm, $^7F_6 \rightarrow {}^5D_2$; 375 nm, $^7F_6 \rightarrow {}^5G_6$), as observed in Figure 7a. Under the excitation of a UV light at 261 nm, the emission spectra of the $NaCeF_4$:mTb^{3+} NRs consist of the transitions of Tb^{3+}: 489 nm, $^5D_4 \rightarrow {}^7F_6$; 543/546 nm, $^5D_4 \rightarrow {}^7F_5$, strongest; 584 nm, $^5D_4 \rightarrow {}^7F_4$; and 620 nm, $^5D_4 \rightarrow {}^7F_3$, respectively. The bright green emissions of the $NaCeF_4$:Tb^{3+} NRs are presented (insets in Figure 8) and the CIE coordinates are calculated to (0.31, 0.51) for $NaCeF_4$:$0.02Tb^{3+}$ and (0.33, 0.54) for $NaCeF_4$:$0.05Tb^{3+}$ NRs. The mono-exponential fitting of the $NaCeF_4$:mTb^{3+} NRs shows the lifetime of the transition ($^5D_4 \rightarrow {}^7F_5$) and the decay times were measured to 7.71 and 8.92 ms for m = 0.05 and 0.1, respectively (shown in Figure 7c). The quantum yields of the $NaCeF_4$:mTb^{3+} NRs was recorded to 25% and 30%, respectively.

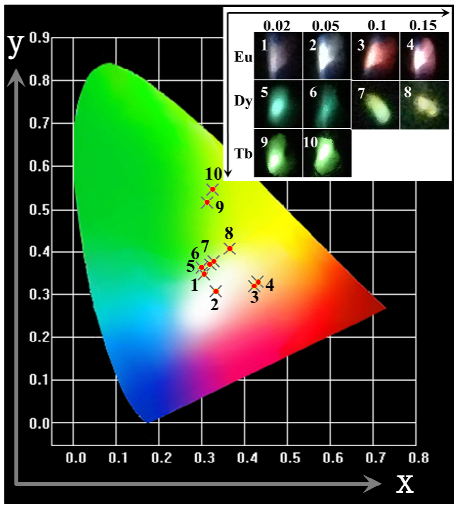

Figure 8. The CIE chromaticity diagram of the as-prepared $NaCeF_4$:Eu^{3+}/Dy^{3+}/Tb^{3+} NRs. The upright insets present the digital photographs of the as-prepared powders under the excitation of a Xe lamp at the corresponding strongest excitation peak.

3.3 CL Properties

The low-voltage CL properties of materials are significant for field-emission displays. To further reveal their potential application in field-emission devices, CL properties were investigated. As shown in Figure 9, their CL spectra were similar to the corresponding PL spectra. Under the low-voltage electron beam excitation (accelerating voltage: 3.15 kV), $NaCeF_4$:$0.15Eu^{3+}$ NRs gives bright yellowish red light with emission peaks centered at 593, 618, and 697 nm, owing to the transitions $^5D_0 \rightarrow {}^7F_1$, $^5D_0 \rightarrow {}^7F_2$, and $^5D_0 \rightarrow {}^7F_4$ of Eu^{3+} respectively. For $NaCeF_4$:$0.02Dy^{3+}$ NRs, the CL spectrum (excitation voltage: 4.75 kV) shows two intense emission peaks at 480 and 572 nm due to the transitions $^4F_{9/2} \rightarrow {}^6H_{15/2}$ and $^4F_{9/2} \rightarrow {}^6H_{13/2}$ of Dy^{3+}, respectively. These NRs show greenish yellow light under the electron beam excitation. As for $NaCeF_4$:$0.05Tb^{3+}$ NRs, the CL spectrum (excitation voltage: 4.75 kV) are composed of emission peaks at 491, 545, 587, and 622 nm, which result from $^5D_4 \rightarrow {}^7F_6$, $^5D_4 \rightarrow {}^7F_5$, $^5D_4 \rightarrow {}^7F_4$, and $^5D_4 \rightarrow {}^7F_3$ of Tb^{3+}, respectively.

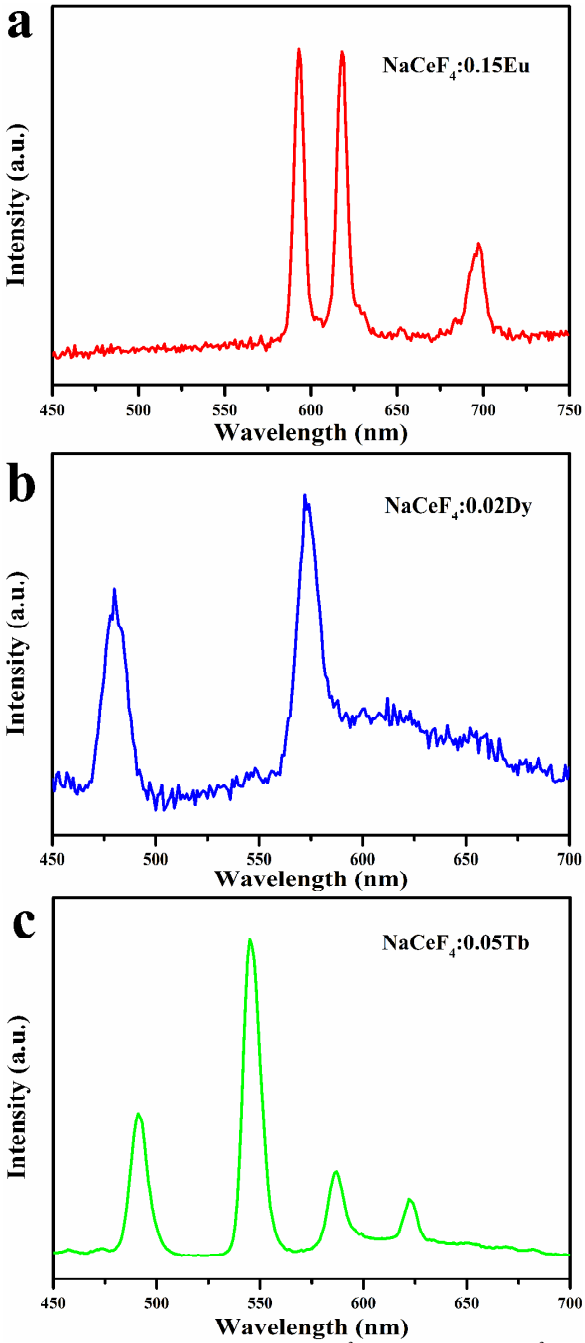

Figure 9. CL spectra of (a) $NaCeF_4$:0.15Eu^{3+}, (b) $NaCeF_4$:0.02Dy^{3+}, and (c) $NaCeF_4$:0.05Tb^{3+} NRs. Accelerating voltages were 3.15, 4.75, and 4.75 kV for a-c, respectively.

4. Conclusion

In summary, the pure hexagonal phase $NaCeF_4$:Ln^{3+} (Ln^{3+} = Eu^{3+}, Dy^{3+}, Tb^{3+}) NRs have been successfully fabricated via a hydrothermal method. The microstructural studies exhibit the formation of high quality $NaCeF_4$:Ln^{3+} NRs with monodispersity, uniform shape and single crystal nature. Furthermore, the tunable multicolor, especially white emissions can be obtained by adjusting the doping ions and the doping contents. Importantly, the CIE coordinates of $NaCeF_4$:0.05Eu^{3+} NRs are located in white region and calculated to (0.33, 0.31), which is closed to the standard white light emission (0.33, 0.33). These findings provide a simple way for white light emission by only doping single Eu^{3+}, which is different with previous demonstrated Ce^{3+}/Mn^{2+} co-doped phosphors. The excellent DC emissions, tunable multicolor output and bright white light luminescence of the $NaCeF_4$:Ln^{3+} NRs may find application in field-emission devices and solid state lighting.

Acknowledgments

This work was supported by the National Natural Science Foundation of China (Nos. 51102202 and 31370736), Specialized Research Fund for the Doctoral Program of Higher Education of China (No. 20114301120006) and Hunan Provincial Natural Science Foundation of China (No. 12JJ4056), and Scientific Research Fund of Hunan Provincial Education Department (13B062).

Notes and references

[a] *College of Physics and Information Science and Key Laboratory of Low-dimensional Quantum Structures and Quantum Control of the Ministry of Education, Hunan Normal University, Changsha 410081, Hunan, China. Email: songjunz@hunnu.edu.cn*

[b] *School of Materials Science and Engineering, Key Laboratory of Low-dimensional Materials and Application Technology (Ministry of Education), Xiangtan University, Xiangtan 411105, People's Republic of China.*

[c] *Materials Research Center and Department of Applied Physics, The Hong Kong Polytechnic University, Hong Kong.*

1. Y. S. Liu, D. T. Tu, H. M. Zhu and X. Y. Chen, *Chem. Soc. Rev.*, 2013, **42**, 6924.
2. S. L. Gai, C. X. Li, P. P. Yang and J. Lin, *Chem. Rev.,* 2014, **114**, 2343.
3. F. Wang, X. J. Xue and X. G. Liu, *Angew. Chem. Int. Ed.*, 2008, **47**, 906.
4. F. Wang and X. G. Liu, *Acc. Chem. Res.*, 2014, **47**, 1378.
5. Y. P. Li, J. H. Zhang, X. Zhang, Y. S. Luo, S. Z. Lu, X. G. Ren, X. J. Wang, L. D. Sun and C. H. Yan, *Chem. Mater.*, 2009, **21**, 468.
6. Y. S. Liu, D. T. Tu, H. M. Zhu, R. F. Li, W. Q. Luo and X. Y. Chen, *Adv. Mater.*, 2010, **22**, 3266.
7. F. Wang, Y. Han, C. S. Lim, Y. H. Lu, J. Wang, J. Xu, H. Y. Chen, C. Zhang, M. H. Hong and X. G. Liu, *Nature*, 2010, **463**, 1061.
8. Y. F. Wang, G. Y. Liu, L. D. Sun, J. W. Xiao, J. C. Zhou and C. H. Yan, *ACS Nano*, 2013, **7**, 7200.
9. N. M. Idris, M. K. Gnanasammandhan, J. Zhang, P. C. Ho, R. Mahendran and Y. Zhang, *Nature Medicine*, 2012, **18**, 1580.
10. G. Y. Chen, T. Y. Ohulchanskyy, R. Kumar, H. Ågren and P. N. Prasad, *ACS Nano*, 2010, **4**, 3163.
11. M. Haase and H. Schäfer, *Angew. Chem. Int. Ed.*, 2011, **50**, 5808.
12. W. P. Fan, B. Shen, W. B. Bu, F. Chen, K. L. Zhao, S. J. Zhang, L. P. Zhou, W. J. Peng, Q. F. Xiao, H. Y. Xing, J. N. Liu, D. L. Ni, Q. J. He and J. L. Shi, *J. Am. Chem. Soc.*, 2013, **135**, 6494.
13. J. C. Boyer, F. Vetrone, L. A. Cuccia and J. A. Capobianco, *J. Am. Chem. Soc.*, 2006, **128**, 7444.
14. X. Wang and Y. D. Li, *Angew. Chem. Int. Ed.*, 2003, **42**, 3497.
15. S. Sivakumar, F. C. J. M. van Veggel and M. Raudsepp, *J. Am. Chem. Soc.*, 2005, **127**, 12464.
16. H. T. Wong, H. L. W. Chan and J. H. Hao, *Appl. Phys. Lett.*, 2009, **95**, 022512.
17. Z. Y. Hou, P. P. Yang, C. X. Li, L. L. Wang, H. Z. Lian, Z. W. Quan and J. Lin , *Chem. Mater.*, 2008, **20**, 6686.
18. S. J. Zeng, Z. G. Yi, W. Lu, C. Qian, H. B. Wang, L, Rao, T. M. Zeng, H. R. Liu, H. J. Liu, B. Fei and J. H. Hao, *Adv. Funct. Mater.*, 2014, DOI: 10.1002/adfm.201304270.

19. J. T. Hu, L. S. Li, W. D. Yang, L. Manna, L. W. Wang and A. P. Alivisatos, *Science*, 2001, **292**, 2060.
20. X. Wang, J. Zhuang, Q. Peng and Y. Li, *Inorg. Chem.*, 2006, **45**, 6661.
21. S. J. Zeng, M. K. Tsang, C. F. Chan, K. L. Wong, B. Fei and J. H. Hao, *Nanoscale*, 2012, **4**, 5118.
22. G. Z. Ren, S. J. Zeng and J. H. Hao, *J. Phys. Chem. C*, 2011, **115**, 20141.
23. J. Zhuang, L. Liang, H. H. Y. Sung, X. Yang, M. Wu, I. D. Williams, S. Feng and Q. Su, *Inorg. Chem.*, 2007, **46**, 5404.
24. C. Feldman, T. Justel, C. R. Ronda and P. J. Schmidt, *Adv. Funct. Mater.*, 2003, **13**, 511.
25. A. Shalav, B. S. Richards, T. Trupke, K. W. Krämer and H. U. Güdel, *Appl. Phys. Lett.*, 2005, **86**, 013505.
26. Y. W. Zhang, X. Sun, R. Si, L. P. You and C. H. Yan, *J. Am. Chem. Soc.*, 2005, **127**, 3260.
27. L. Y. Wang and Y. D. Li, *Chem. Commun.*, 2006, 2557.
28. Z. Q. Li and Y. Zhang, *Angew. Chem., Int. Ed.*, 2006, **45**, 7732.
29. L. Y. Wang, R. X. Yan, Z. Y. Hao, L. Wang, J. H. Zeng, H. Bao, X. Wang, Q. Peng and Y. D. Li, *Angew. Chem., Int. Ed.*, 2005, **44**, 6054.
30. H. K. Liu, Y. Luo, Z. Y. Mao, L. B. Liao and Z. G. Xia, *J. Mater. Chem. C*, 2014, **2**, 1619.
31. M. M. Jiao, Y. C. Jia, W. Lü, W. Z. Lv, Q. Zhao, B. Q. Shao and H. P. You, *J. Mater. Chem. C*, 2014, **2**, 90.
32. D. L. Geng, M. M. Shang, Y. Zhang, H. Z. Lian and J. Lin, *Inorg. Chem.*, 2013, **52**, 13708.
33. M. M. Jiao, N. Guo, W. Lü, Y. C. Jia, W. Z. Lv, Q. Zhao, B. Q. Shao, and H. P. You, *Inorg. Chem.*, 2013, **52**, 10340.
34. W. H. Di, X. G. Ren, H. F. Zhao, N. Shirahata, Y. Sakka and W. P. Qin, *Biomaterials*, 2011, **32**, 7226.
35. J. C. Boyer, J. Gagnon, L. A. Cuccia and J. A. Capobianco, *Chem. Mater.*, 2007, **19**, 3358.
36. J. H. Zeng, Z. H. Li, J. Su, L. Wang, R. Yan and Y. Li, *Nanotechnology*, 2006, **17**, 3549.
37. X. S. Qu, H. K. Yang, G. H. Pan, J. W. Chung, B. K. Moon, B. C. Choi and J. H. Jeong, *Inorg. Chem.*, 2011, **50**, 3387.
38. J. W. Stouwdam and F. C. J. M. van Veggel, *Langmuir*, 2004, **20**, 11763.
39. G. Blasse and B. C. Grabmaier, *Luminescent Materials*; Springer: Berlin, 1994.
40. M. Yu, J. Lin and J. Fang, *Chem. Mater.*, 2005, **17**, 1783.
41. S. Li, T. Xie, Q. Peng and Y. Li, *Chem. Eur. J.*, 2009, **15**, 2512.
42. S. J. Zeng, J. J. Xiao, Q. B. Yang and J. H. Hao, *J. Mater. Chem.*, 2012, **22**, 9870.
43. X. Wang, J. Zhuang, Q. Peng and Y.D. Li, *Nature*, 2005, **437**, 121.
44. S. J. Zeng, H. B. Wang, W. Lu, Z. G. Yi, L. Rao, H. R. Liu and J. H. Hao, *Biomaterials*, 2014, **35**, 2934.
45. K. W. Kramer, D. Biner, G. Frei, H. U. Gudel, M. P. Hehlen and S. R. Luthi, *Chem. Mater.*, 2004, **16**, 1244.
46. R. D. Shannon, *Acta Cryst.*, 1976, **A32**, 751.
47. F. Wang, X. P. Fan, M. Q.Wang and Y. Zhang, *Nanotechnology*, 2007, **18**, 025701.
48. G. Blasse and N. Sabbatini, *Mater. Chem. Phys.*, 1987, **16**, 237.
49. G. Blasse, *Phys. Status Solidi.*, 1983, **75**, K41.
50. D. L. Dexter and J. A. Schulman, *J. Chem. Phys.*, 1954, **22**, 1063.
51. G. Blasse, *Philips Res. Rep.*, 1969, **24**, 131.
52. A. K. Parchur, R. S. Ningthoujam, S. B. Rai, G. S. Okram, R. A. Singh, M. Tyagi, S. C. Gadkari, R. T. and R. K. Vatsa, *Dalton Trans.*, 2011, **40**, 7595.
53. B. P. Singh, A. K. Parchur, R. S. Ningthoujam, A. A. Ansari, P. Singha and S. B. Rai, *Dalton Trans.*, 2014, **43**, 4779.
54. A. K. Parchur, A. A. Ansari, B. P. Singh, T. N. Hasan, N. A. Syed, S. B. Raia and R. S. Ningthoujam, *Integr. Biol.*, 2014, **6**, 53.
55. Y. Zhang, G. G. Li, D. L. Geng, M. M. Shang, C. Peng and J. Lin, *Inorg. Chem.*, 2012, **51**, 11655.
56. M. M. Shang, D. L. Geng, D. M. Yang, X. J. Kang, Y. Zhang and J. Lin, *Inorg. Chem.*, 2013, **52**, 3102.